

**Highlighting research from Uppsala University,
Dept. Physics & Astronomy, Div. Röntgenfysik.**

Wafer-sized WS₂ monolayer deposition by sputtering

Tungsten disulphide (WS₂) with thicknesses ranging from monolayer (ML) to several monolayers can be grown on SiO₂/Si, Si, and Al₂O₃ by pulsed direct current-sputtering. Sputter deposition is a scalable process and here it is demonstrated that wafer-scale deposition of a 2D transition metal dichalcogenide monolayer can be achieved in this manner. Growing 2D layers directly by sputtering opens up the way for designing 2D materials and batch production of high-uniformity and high-quality (stoichiometric, large grain sizes, flatness) WS₂ films, which will advance their practical applications in various fields.

As featured in:



See Andreas Lindblad *et al.*,
Nanoscale, 2022, **14**, 6331.



Cite this: *Nanoscale*, 2022, **14**, 6331

Wafer-sized WS₂ monolayer deposition by sputtering

Michelle Marie S. Villamayor,^a Sajid Husain,^{b,c} Reinier Oropesa-Nuñez,^b Fredrik O. L. Johansson,^d Rebecka Lindblad,^e Pedro Lourenço,^f Romain Bernard,^f Nadine Witkowski,^f Geoffroy Prévot,^f Nomi L. A. N. Sorgenfrei,^{g,h} Erika Giangrisostomi,^g Alexander Föhlisch,^{g,h} Peter Svedlindh,^b Andreas Lindblad^{*d} and Tomas Nyberg^a

We demonstrate that tungsten disulphide (WS₂) with thicknesses ranging from monolayer (ML) to several monolayers can be grown on SiO₂/Si, Si, and Al₂O₃ by pulsed direct current-sputtering. The presence of high quality monolayer and multilayered WS₂ on the substrates is confirmed by Raman spectroscopy since the peak separations between the A_{1g}-E_{2g} and A_{1g}-2LA vibration modes exhibit a gradual increase depending on the number of layers. X-ray diffraction confirms a textured (001) growth of WS₂ films. The surface roughness measured with atomic force microscopy is between 1.5 and 3 Å for the ML films. The chemical composition WS_x (x = 2.03 ± 0.05) was determined from X-ray Photoelectron Spectroscopy. Transmission electron microscopy was performed on a multilayer film to show the 2D layered structure. A unique method for growing 2D layers directly by sputtering opens up the way for designing 2D materials and batch production of high-uniformity and high-quality (stoichiometric, large grain sizes, flatness) WS₂ films, which will advance their practical applications in various fields.

Received 21st December 2021,
 Accepted 10th March 2022

DOI: 10.1039/d1nr08375a

rsc.li/nanoscale

1. Introduction

Monolayer two dimensional (2D) transition metal dichalcogenides (TMDCs) recently gained attention due to their excellent electrical, optical and magnetic properties.^{1,2} Because of their semiconducting characteristics, TMDCs provide the possibility to overcome the shortcomings of zero-bandgap materials, like graphene. Tungsten disulfide (WS₂) is one of the most studied 2D-TMDCs, and is a layered material similar to graphene. A

layer of a TMDC is typically 6–8 Å thick and consists of one plane of metal atoms sandwiched between two planes of chalcogen atoms – in the planes, the atoms are arranged in hexagonal patterns. Consecutive layers are held together by weak van der Waals forces. Whereas bulk WS₂ has an indirect band gap of 1.3 eV, a monolayer has a direct band gap reported to be slightly lower than 2.05 eV since the direct electronic transitions in WS₂ originate from excitonic radiative relaxation.^{3,4} FET devices based on monolayer WS₂ exhibit an excellent ON/OFF current ratio of 10⁸ and carrier mobility greater than 200 cm² V⁻¹ (s⁻¹).⁵ The strong photoluminescence of WS₂ makes it a possible component for future electronic and optoelectronic devices. Its potential applications include transistors, lithium-ion batteries, solid lubricants, chemical sensors, membranes, heterogeneous catalysis especially for the hydrogen evolution reaction (HER) in photocatalytic water splitting, and spintronics.^{6,7}

Several methods can be used to grow WS₂ films on various substrates. Chemical vapor deposition (CVD) is the most common process to grow TMDCs.^{8–15} However related methods, including atomic layer deposition (ALD)^{6,16} and metal-organic CVD (MOCVD)^{7,17,18} have been used. Also exfoliation of monolayer, or few layers of a dichalcogenide have been achieved.^{10,19}

The biggest issue of these methods is that they are unsuitable for the growth of large area films. They produce small areas, or even flake sizes in the case of exfoliation methods.²⁰

^aDivision of Solid State Electronics, Department of Electrical Engineering, Uppsala University, Box 65, SE-751 03 Uppsala, Sweden

^bDivision of Solid State Physics, Department of Materials Science and Engineering, Uppsala University, Box 35, SE-751 03 Uppsala, Sweden

^cUnité Mixte de Physique, CNRS, Thales, Université Paris-Saclay, 91767 Palaiseau, France

^dDivision of X-ray Photon Science, Department of Physics & Astronomy, Uppsala University, Box 516, SE-751 20 Uppsala, Sweden
 E-mail: andreas.lindblad@physics.uu.se

^eDivision of Inorganic Chemistry, Department of Chemistry-Ångström, Uppsala University, Box 521, SE-751 20 Uppsala, Sweden

^fSorbonne Université, CNRS, Institut des NanoSciences de Paris, INSP, F-75005 Paris, France

^gInstitute for Methods and Instrumentation for Synchrotron Radiation Research, Helmholtz-Zentrum Berlin für Materialien und Energie GmbH, Albert-Einstein-Straße 15, 12489 Berlin, Germany

^hInstitut für Physik und Astronomie, Universität Potsdam, Karl-Liebknecht-Straße 24/25, 14476 Potsdam, Germany



Xu *et al.*, have reported large-scale deposition of monolayer WS₂ on SiO₂/Si substrate that resulted in triangular flakes with 12.7 μm sides.¹² Another approach is to sputter from a W target and then post-anneal the metal film in sulfur atmosphere.¹⁴

A two-stage process has been developed to prepare high quality bilayer TMDC stacking using reverse-flow chemical vapor epitaxy.²¹ Recently, Zhang and co-workers²² succeeded in 6-inch wafer size growth of TMDCs *e.g.* MoS₂. Monolayers of MoS₂ were grown using a low pressure face-to-face precursor CVD method where the Mo sheet is kept in front of a soda-lime glass substrate. This process allows large-scale wafer size TMDC production. However, during transfer of the TMDCs onto a different substrate, large strain and cracks develop – a shortcoming of this indirect growth method. High quality TMDCs were also successfully deposited on SiO₂ substrates using a two-step process where a metal film is deposited on a substrate followed by sulfurization.^{23,24}

Monolayer TMDC films can be produced by CVD, MOCVD and ALD as outlined above. For instance, wafer-sized specimens synthesised by these techniques are available commercially.

Several attempts have been made to grow TMDCs using sputtering, including MoS₂²⁵ and WS₂²⁶ on various substrates such as sapphire Al₂O₃, glass, and Si/SiO₂, but issues relating to film quality when grown on Si/SiO₂ substrates have been reported. To grow WS₂ films, Regula *et al.* have used a sintered WS₂ target in Ar/H₂S atmosphere (H₂S 0–10%), where the substrate was electrically grounded, and heated at 600 °C at a process pressure between 7.5–9 mTorr.²⁷ The group of Ellmer explored the effect of different process parameters (substrate temperature, amount of reactive gas, sputtering pressure, substrate material, process gas) using a W target for sputter depositing WS₂.^{28,29} Process parameters for growth of multilayer WS₂ films by sputtering from a WS₂ have been reported earlier by our group.³⁰

The sputtering technique is a versatile and promising method for cost-efficient large scale industrial production of TMDCs – a scope unavailable to, *e.g.* the resource intensive CVD-technique.

Synthesizing TMDC monolayers over large areas (wafer-scale) using sputtering techniques would thus be a route providing industrially viable application of these materials. Tao *et al.*, deposited MoS₂ monolayers by sputtering of Mo together with evaporated sulphur.²⁵ To our knowledge, no one has produced a large scale monolayer TMDC by sputtering from a TMDC target without co-evaporation or post-processing (*e.g.* sulphurization or annealing).

In this paper we report on high quality WS₂ large area monolayers directly grown on 500 nm SiO₂ on Si, Si, and sapphire substrates. We have used a WS₂ target together with H₂S atmosphere as described below. The quality of the films has been verified by several methods: Raman spectroscopy, atomic force microscopy (AFM), photoluminescence (PL), cross sectional transmission electron microscopy (TEM), X-ray diffraction (XRD) and X-ray photoelectron spectroscopy (XPS).

2. Methods

2.1. Film preparation

WS₂ films were deposited using a CS 600 von Ardenne high vacuum magnetron sputtering system. The magnetron was located on the top lid of the deposition chamber with a 45° angle towards the substrate table at the center of the chamber bottom shown as shown in Fig. 1(a). The target-substrate distance was fixed to 16 cm. Substrates (SiO₂/Si, Si and Al₂O₃) were located in front of the target and heated to 700 °C during deposition.

The base pressure was 10⁻⁷ Torr for all depositions. A 100 mm WS₂ target (99.9% purity, K. Lesker, Inc.) was powered with a 200 W pulsed-DC at 20 kHz frequency. The working pressure was kept constant at 50 mTorr with H₂S flow rate of 20 sccm. The deposition time for one monolayer WS₂ was around 2 minutes resulting in a film covering a whole 4 inch wafer as shown in Fig. 1(b).

2.2. Characterization

2.2.1. Raman spectroscopy and photoluminescence. Raman spectra were recorded with a micro Raman spectrometer in-Via Renishaw Raman microscope using 532 nm laser wavelength. Measurements were performed with 10% of 20 mW max power to avoid damaging the sample due to laser heating. In order to determine the quality of the grown film, peak separation Raman mapping was taken from the A_{1g} and E_{2g} peak positions. The Raman signal was calibrated using the signal from substrate Si. We do not observe features from SiO₂ owing to the low intensity of from the amorphous phase.³⁶ Further, the same laser wavelength with 5% power was used to record the photoluminescence (PL) spectra on the monolayer and bilayer samples. The spot size for the measurements was 1 μm (using a 50×/0.75 objective).

2.2.2. X-ray photoelectron spectroscopy (XPS). XPS measurements were performed using a PHI Quantera II scanning XPS microprobe equipped with monochromatic Al K_α radiation (1486.7 eV). A spot size of 100 μm, and a photoelectron take-off angle of 45° were used. The setup is regularly calibrated using reference samples of Ag, Au and Cu according to the ISO standard 15472.³⁷ Chemical compositions were

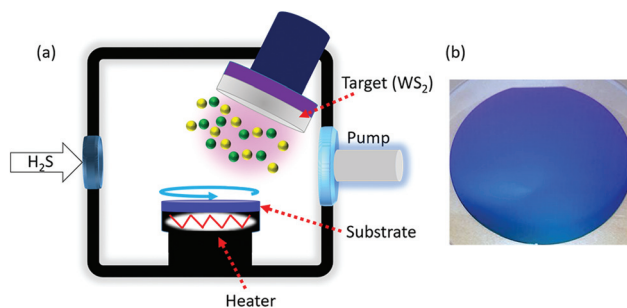


Fig. 1 (a) Schematic diagram of the sputter source used to deposit a monolayer and few layers of WS₂. (b) A 4-inch diameter wafer with 1 monolayer WS₂ on SiO₂ substrate.



obtained by fitting the W 4f and S 2p core level spectra using Voigt functions after removing a Tougaard background, and by using setup-specific sensitivity factors to account for *e.g.*, photoionization cross sections.

2.2.3. Atomic force microscopy (AFM). The AFM images were acquired using a Bruker Dimension Icon atomic force microscope (Bruker Dimension IconTM, Billerica, MA, USA). Silicon RTESPA-300 cantilevers (Bruker, Billerica, MA, USA) having a nominal tip diameter of 8 nm were used to perform the AFM measurements. Intermittent contact mode AFM images (1024×1024 data points) of $1 \mu\text{m} \times 1 \mu\text{m}$ by keeping the working set point above 70% of the free oscillation amplitude was employed. A scan rate of 0.5 Hz was used for the acquisition of the images. The Gwyddion 2.54 software was used to process the images and characterize the roughness of WS₂ coatings on three different substrates (SiO₂/Si, Si, and Al₂O₃).

2.2.4. X-Ray diffraction (XRD). The X-ray diffraction patterns of films consisting of 8 monolayers (8 ML) deposited on SiO₂/Si, Si and Al₂O₃ substrates were recorded with a Phillips X'pert MRD diffractometer using Cu K α radiation (spot size $1.4 \text{ mm} \times 10 \text{ mm}$). These were measured in θ - 2θ mode. Further, the in-plane measurements were performed on a Rigaku SmartLab diffractometer with a 9 kW rotating Cu anode with a $5 \text{ mm} \times 5.7 \text{ mm}$ spot size.

3. Results and discussion

3.1. Raman spectroscopy

In WS₂ the first order phonon modes that occur at the Brillouin zone centre (Γ) are: A_{1g}, 2A_{2u}, 2B_{2g}, B_{1u}, E_{1g}, 2E_{1u},

2E_{2g}, and, E_{2u}. A_{2u} and E_{1u} are acoustic modes and infrared active. A_{1g}, E_{1g}, and E_{2g}, are Raman active. B_{2g}, B_{1u}, and E_{2u} are undetected optically. In addition to these, a longitudinal acoustic (LA) mode at the (M) symmetry point of the Brillouin zone exists in these TMDCs due to the collective in-plane movement of the atoms in the lattice.³⁸ Note that the 2LA is the second harmonic mode³⁹ appear due to the laser excitation and it can reduce with laser wavelength.³⁸ Moreover, the 2LA intensity is suppressed in more than one layer of WS₂, which confirmed the higher layer numbers of WS₂ (discussed later). The LA mode overlaps at the Γ point with the E_{2g} mode.

Fig. 2 shows the Raman spectra recorded on monolayer and few layers WS₂. The peak positions are extracted by multi-peak least squares fit of Lorentzian peaks to the data. These Raman spectra mainly show A_{1g} at $418.27 \pm 0.06 \text{ cm}^{-1}$, E_{2g} at $358.50 \pm 0.11 \text{ cm}^{-1}$, and 2LA at $354.42 \pm 0.42 \text{ cm}^{-1}$. The uncertainty in the peak position is the standard error obtained from the least squares multi-peak fit. These peak positions are representative of monolayer of WS₂ at 300 K.⁴⁰ Notice that low intensity peaks observed at low wavenumber around 300 and 325 cm^{-1} correspond to the out-of-plane acoustic phonon modes ascribed to the edge of the M-point in the Brillouin zone.⁴¹

When we increase the number of WS₂ layers, the peak positions are shifted with growing peak separation. For bilayer WS₂, peak positions for A_{1g}, E_{2g}, and 2LA are observed at $418.27 \pm 0.06 \text{ cm}^{-1}$, $356.37 \pm 0.13 \text{ cm}^{-1}$, and $350.9 \pm 0.37 \text{ cm}^{-1}$, respectively. Further increasing the number of WS₂ layers increases the peak separation as shown in Fig. 2(e) and (f) for A_{1g}-2LA and A_{1g}-E_{2g}, respectively. This peak separation indicates the formation of one, two, and so on layers towards bulk WS₂. Comparably, our results agree with those of Shi *et al.*,⁴⁰

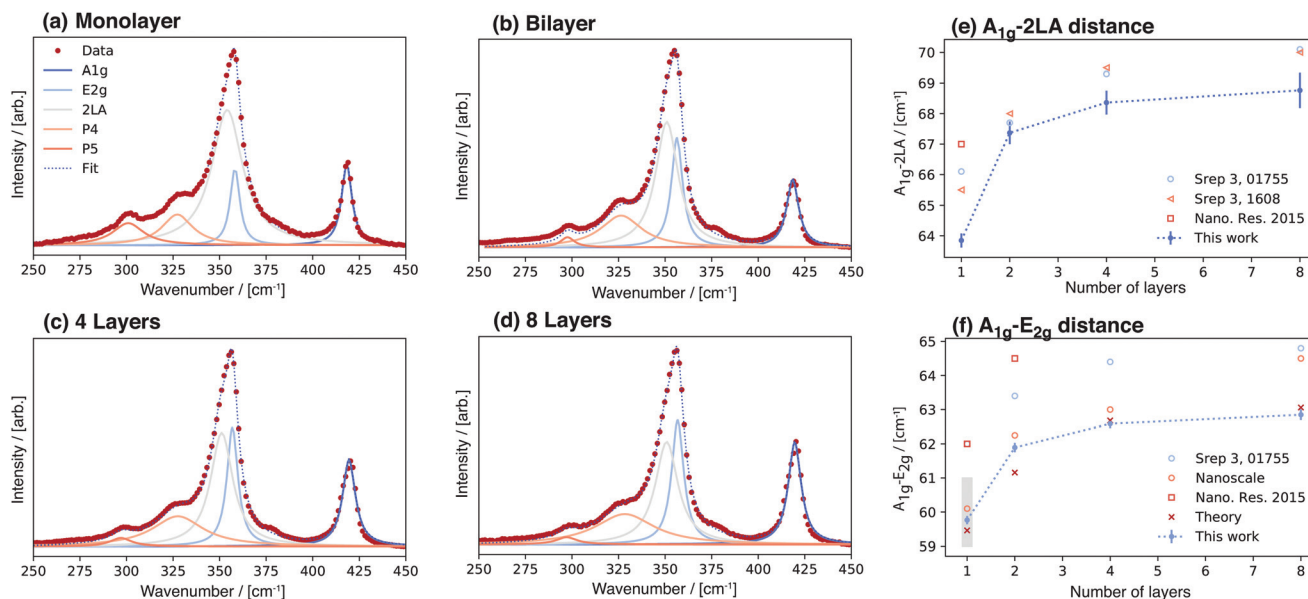


Fig. 2 Raman spectra as a function of number of layers recorded on: (a) a monolayer (1ML), (b) bilayer (2ML), (c) four layer (4ML), and (d) eight layer (8ML), sample. (e) Peak separation A_{1g}-2LA, and (f) A_{1g}-E_{2g}. The theory data points are from ref. 31, experimental data: blue circles,³² red circles,³³ red squares,³⁴ red triangles,³⁵ The grey rectangle in (f) indicate the observed peak separations in the Raman mapping discussed in the text and shown in Fig. 4.



and theoretical predictions³¹ rather than earlier experimental reports of peak separations of WS₂ on monolayer to bulk samples.^{34,35,38,42} The peak intensity ratio is calculated as shown in Fig. 3. Relative intensity ratios of the 2LA and A_{1g} phonon modes for mono- and bi-layer samples agrees with reported results.³⁸ An intensity ratio close to 2 indicates the presence of a monolayer.⁴¹

In order to determine the film uniformity, Raman mapping was performed on a 60 × 60 mm² area of a 4-inch SiO₂/Si wafer. Fig. 4 shows the map of the separation between the two peak positions of A_{1g}–E_{2g}. The map indicate that the thickness is uniform over the whole 4-inch wafer. Raman mapping shows a narrow spread of the spacing around the value expected for a monolayer (59.9 cm⁻¹). The peak separation is within the spread indicated with a grey rectangle in Fig. 2(f).

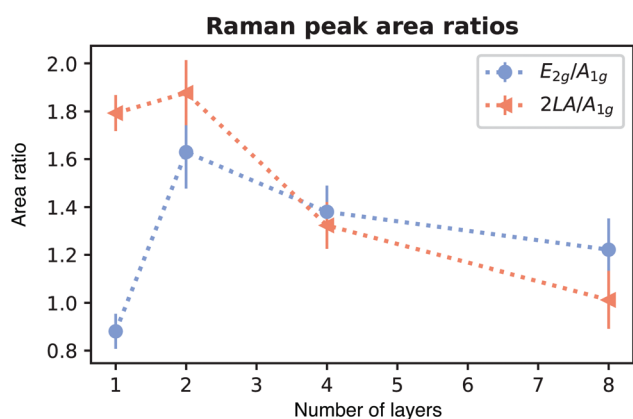


Fig. 3 Peak intensity ratio of E_{2g}, A_{1g}, and 2LA as function of number of layers.

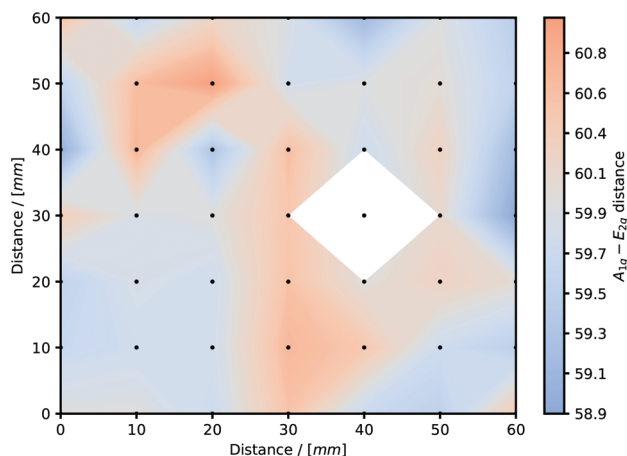


Fig. 4 (a) Raman mapping showing peak separation of A_{1g}–E_{2g} on very large area monolayer WS₂ sample on SiO₂/Si. The peak separations were measured every 10 mm over area of 60 × 60 mm² here presented with the points linearly interpolated. The black dots indicate where the peak separations have been measured. The white area is centered on a position where no data was acquired. The range is represented by the gray rectangle in Fig. 2(f).

The mapping thus exhibits a high quality monolayer growth on a large area substrate. This demonstrates the industrial compatibility of WS₂ directly grown on SiO₂ substrates.

3.2. Photoluminescence (PL) spectroscopy

Fig. 5 shows the photoluminescence spectra of monolayer and bilayer WS₂ grown on SiO₂ substrate. The main peak is centered at 2.03 eV for the monolayer sample. The small peaks at 2.17 eV to 2.20 eV are Raman modes. There was significantly smaller photoluminescence signal observed for the bilayer sample. These observations agree with previous computations and experimental results.^{3,4,35,43–48}

3.3. X-Ray photoelectron spectroscopy (XPS)

The core level photoelectron spectra recorded on WS₂ monolayer grown on SiO₂ substrates are shown in Fig. 6. A survey spectrum is shown in the bottom panel where we identify signatures at binding energies from: overlayer W, S (corresponding to WS₂ binding energies⁴⁹); substrate Si and O (at SiO₂ binding energy positions⁵⁰) and C species adsorbed on the surface⁵¹ – we also find trace amounts of Ag.⁵² The horizontal lines indicate the distance from the main peak to the plasmon excitation.^{53,54} The C 1s core level (at binding energy 284 eV) do not have a plasmon which indicate that this element is weakly adsorbed on the surface.

The recorded spectra have been fitted with spin-orbit components for the W 4f and S 2p-core levels. The peaks corresponding to the W 5p_{3/2}, W 4f_{5/2}, and W 4f_{7/2} orbitals are observed at 37.9, 34.6 and 32.5 eV, respectively. The peak position of W 4f_{7/2} (32.5 eV) is at larger binding energy compared to metallic W 4f_{7/2} (31.6 eV). For sulfur, the 2p_{1/2} and 2p_{3/2} binding energies are at 163.3 eV 162.1 eV respectively. The binding energies indicate the valence state of the material, and are consistent with a 4⁺ valence state of tungsten, corresponding to a S:W ratio of 2, *i.e.* stoichiometric WS₂.¹⁵ The chemical composition WS_x (x = 2.03 ± 0.05) was obtained from

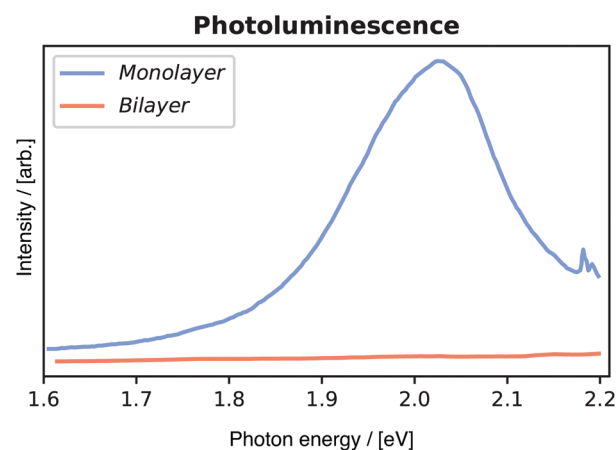


Fig. 5 The PL spectrum of the WS₂ monolayer (black) has its peak intensity at 2.03 eV. No significant PL peak was observed for the bilayer sample (red).



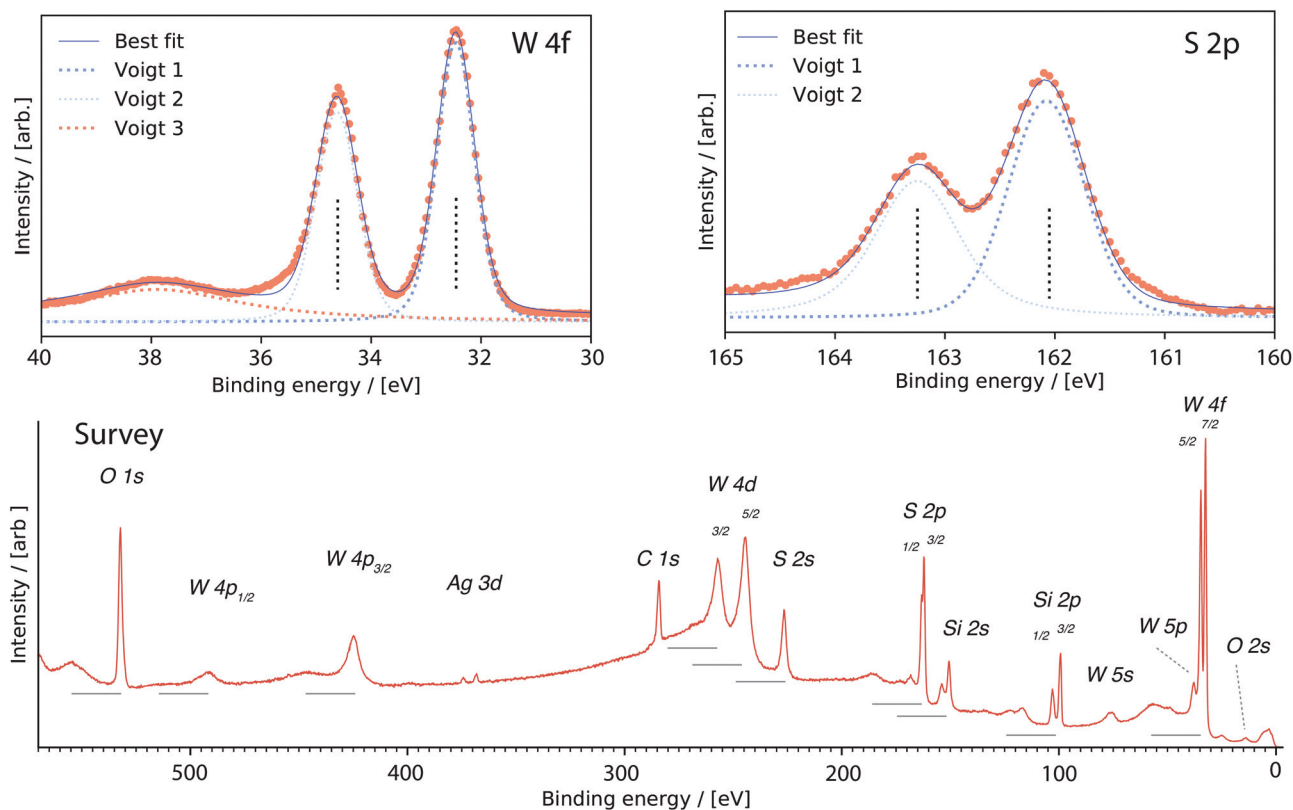


Fig. 6 X-ray photoelectron spectra of sputter-deposited WS₂ monolayer (orange circles). The W 4f-core level spectrum is to the left and the S 2p-core level spectrum to the right. The components from a least squares fit to the data are also included. The positions of the spin orbit components are indicated with vertical lines. A survey spectrum is presented at the bottom with assignment of the core levels. Horizontal lines indicate the distance in energy from a main line to the plasmon peaks discussed in the text.

a least squares fit to the data (Fig. 6). Compared with thicker films obtained using the same deposition parameters for which the S/W ratio was found equal to 1.86,³⁰ monolayer films are thus found to be stoichiometric.

3.4. Atomic force microscopy (AFM)

Fig. 7 displays the topography of the WS₂ films on the SiO₂/Si, Si, Al₂O₃ substrates using AFM. The measured surface roughness σ_a is also indicated on each sample. On the SiO₂/Si substrate, monolayer films present an atomically smooth surface (surface roughness, 3 Å). The roughness increases slightly with increasing number of layers (1 to 8 layers) – for a 8 layer film, we measured a surface roughness of 7 Å. Monolayers with small roughness are also found in the case of Si and Al₂O₃ sub-

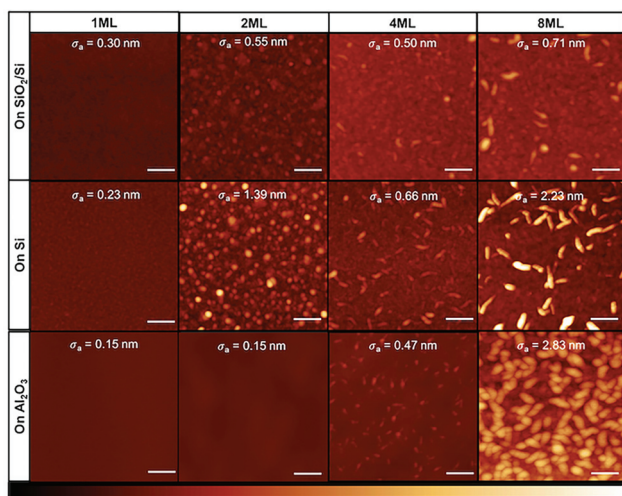


Fig. 7 Topographical analysis from AFM of WS₂ deposited on SiO₂/Si, Si, and Al₂O₃ substrates and the measured surface roughness σ_a . (Scale bar: 200 nm; Z scale: 25 nm.)

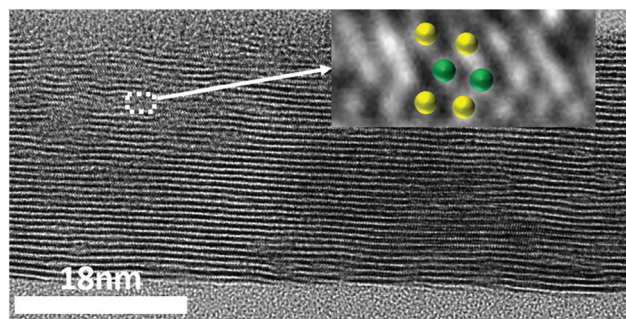


Fig. 8 High resolution cross-sectional TEM image of several layers of WS₂. Inset is zoomed area of one monolayer WS₂ marked by spheres of different colors: green (W) and yellow (S).



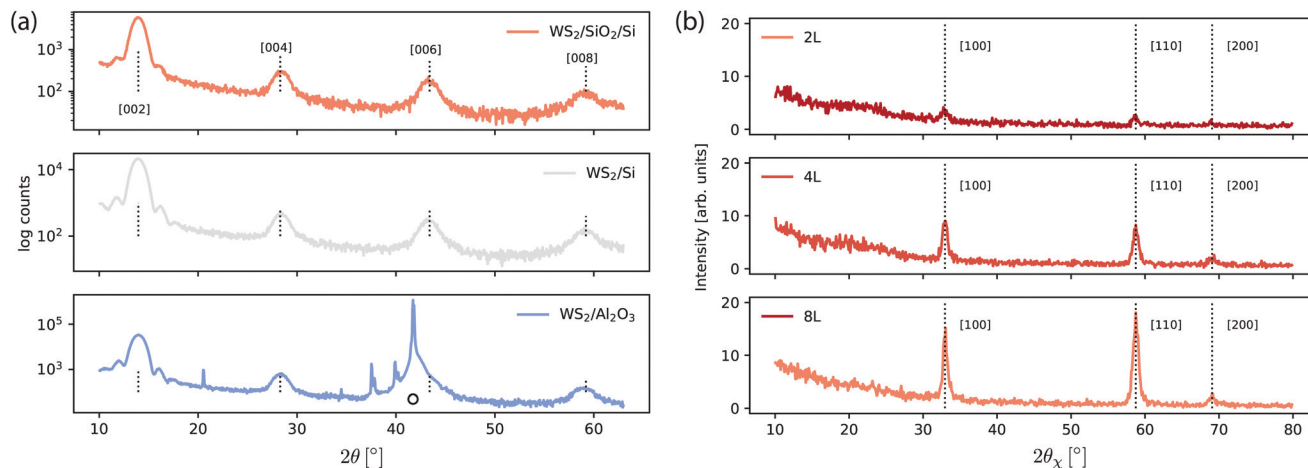


Fig. 9 (a) X-ray diffraction patterns of 8 monolayers of WS₂ deposited on different substrates. The main substrate peak is indicated by a solid circle (peaks at 20, 35, 38 and 40 degrees are also from the substrate). (b) In-plane X-ray diffraction patterns of 2, 4 and 8 monolayers of WS₂/SiO₂/Si.

strates. However, increasing the number of WS₂ layers leads to a significant increase in the surface roughness on Si and Al₂O₃ substrates. On those substrates, layers grow rougher than those grown on SiO₂/Si (top row in Fig. 7). Note that on the Al₂O₃ substrate the bi-layer have a small surface roughness compared to the other bilayers. For bulk thicknesses, grain-like features that add to the to the larger surface roughness are observed.

From this analysis, we can understand that the growth is highly substrate dependent. It is visible that W and S atoms easily bond together when deposited on SiO₂ substrate which follow layer by layer growth even in the bulk regime, Fig. 7 (top panel 8ML). Layer by layer growth also occur on Al₂O₃ substrate up to three layers, but island formation starts after four layers as shown in Fig. 7 (bottom panel 8ML). In case of Si, the growth is mixed, where the small flakes are formed in high number layers with layer-like growth. Thus it is clear that the TMDC growth is substrate dependent which was also observed previously,⁵⁵ and also depends on deposition conditions.³⁰

3.5. Transmission electron microscopy (TEM)

To further verify the layer-by-layer growth and thickness of WS₂ layers, high resolution cross-sectional TEM imaging was performed on a thick film shown in Fig. 8. The total thickness of this film is 26 nm. The thickness of each layer of WS₂ was found to 7 Å. A zoomed cross section is shown in the inset with atomic positions marked with colored spheres, green for W and yellow for S.

3.6. X-Ray diffraction

Fig. 9(a) shows the XRD spectra for 8 monolayer WS₂ film deposited on SiO₂/Si, Si and Al₂O₃ substrates. All the films exhibit a strong orientation along the (001) direction which indicate the crystalline nature of WS₂ growth on all different substrates. The intensity of the [002] peak is highest for the Al₂O₃, followed by that on the Si, and then the SiO₂/Si sub-

strate. The peak positions are identically matched with the commercially available high quality single crystal.⁵⁶ Fig. 9(b) shows the in-plane XRD pattern for 2, 4 and 8 monolayers of WS₂ film deposited on SiO₂/Si. The in-plane lattice constant evolves from 0.3151 nm for the 2 ML thick film to 0.3140 nm for the 8 ML thick film.

The in plane measurements indicate the presence of polycrystalline flakes with domain sizes of the order of 10–20 nm – estimated from using the Scherrer equation and the FWHM of the [100] peak with shape factor 0.9.⁵⁷

4. Conclusions

We have successfully grown stoichiometric monolayer (and multilayer) films of WS₂ on wafer-size substrates of SiO₂/Si, Si and Al₂O₃. The stoichiometry of the film was verified by XPS and the uniformity by Raman mapping. The (001) texture of the WS₂ films is confirmed using X-ray diffraction analysis for all substrates. Raman spectroscopy and Photoluminescence measurements discriminate between the deposition of monolayer and few layers WS₂. Atomic Force Microscopy shows the uniform growth and the atomic smoothness of the layers. The growth of WS₂ is substrate dependent, where monolayer and few layers are formed with layer-by-layer growth. However, islands are formed for large WS₂ film thickness when grown on Al₂O₃ substrate.

Previous attempts to sputter stoichiometric 2D WS₂ films have resulted in slightly substoichiometric films.^{27–30} Stoichiometric films, as produced here, are the result of post-deposition sulfurization caused by H₂S in the chamber during cooling of the substrate. Complete sulfurization is possible since the deposited films are extremely thin in this study.

To summarise: large area monolayer WS₂ films have been grown with a scalable industrially compatible sputter process. This is proof-of-principle of a new route that is complementary to exfoliated and CVD-grown WS₂ (and other TMDC) films.



Conflicts of interest

There are no conflicts to declare.

Acknowledgements

The authors would like to acknowledge Lars Riekehr for the TEM images, Tomas Edvinsson for conducting the preliminary PL measurements, and Yunlin Zheng for XRD measurements. This work was supported by the FLAG-ERA grant for the Layered Metal Sulfides (LaMeS) project by the Swedish Research Council (VR Grant 2017-06816); by the French National Research Agency grant ANR-17-GRF1-0001-03 and by the Carl Tryggers Foundation contract CTS 19:258. A. L. acknowledges the support from the Swedish Research Council (Grants No. 2014-6463 and 2018-05336) and Marie Skłodowska Curie Actions (Cofund, Project INCA 600398). A. F. acknowledges funding by FLAG-ERA Graphene Basic Research 2 2017 in project LaMeS DFG project number 400335214. S. H. and P. S. acknowledges Carl Tryggers Stiftelse for Vetenskaplig Forskning (grant no: CTS 17:450) for the financial support. Reinier Oropesa-Nuñez acknowledges Olle Engkvist (project number: 194-0644) for the financial support.

References

- 1 S. Manzeli, D. Ovchinnikov, D. Pasquier, O. V. Yazyev and A. Kis, *Nat. Rev. Mater.*, 2017, **2**, 17033.
- 2 S. Husain, R. Gupta, A. Kumar, P. Kumar, N. Behera, R. Brucas, S. Chaudhary and P. Svedlindh, *Appl. Phys. Rev.*, 2020, **7**, 041312.
- 3 H. R. Gutiérrez, N. Perea-López, A. L. Elías, A. Berkdemir, B. Wang, R. Lv, F. López-Urías, V. H. Crespi, H. Terrones and M. Terrones, *Nano Lett.*, 2013, **13**, 3447–3454.
- 4 S. Y. Choi, C. T. Yip, G. C. Li, D. Y. Lei, K. H. Fung, S. F. Yu and J. Hao, *AIP Adv.*, 2015, **5**, 067148.
- 5 A. Rawat, N. Jena, S. Dimple and A. De Sarkar, *J. Mater. Chem. A*, 2018, **6**, 8693–8704.
- 6 S. Yeo, D. K. Nandi, R. Rahul, T. H. Kim, B. Shong, Y. Jang, J.-S. Bae, J. W. Han, S.-H. Kim and H. Kim, *Appl. Surf. Sci.*, 2018, **459**, 596–605.
- 7 S. Cwik, D. Mitoraj, O. Mendoza Reyes, D. Rogalla, D. Peeters, J. Kim, H. M. Schütz, C. Bock, R. Beranek and A. Devi, *Adv. Mater. Interfaces*, 2018, **5**, 1–11.
- 8 Y.-H. Lee, X.-Q. Zhang, W. Zhang, M.-T. Chang, C.-T. Lin, K.-D. Chang, Y.-C. Yu, J. T.-W. Wang, C.-S. Chang, L.-J. Li, *et al.*, *Adv. Mater.*, 2012, **24**, 2320–2325.
- 9 A. Alharbi and D. Shahrjerdi, *Appl. Phys. Lett.*, 2016, **109**, 193502.
- 10 Q. Fu and B. Xiang, *Prog. Nat. Sci.: Mater. Int.*, 2016, **26**, 221–231.
- 11 G. V. Bianco, M. Losurdo, M. M. Giangregorio, A. Sacchetti, P. Prete, N. Lovergine, P. Capezzuto and G. Bruno, *RSC Adv.*, 2015, **5**, 98700–98708.
- 12 Z. Xu, Y. Lv, J. Li, F. Huang, P. Nie, S. Zhang, S. Zhao, S. Zhao and G. Wei, *RSC Adv.*, 2019, **9**, 29628–29635.
- 13 B. Groven, D. Claes, A. Nalin Mehta, H. Bender, W. Vandervorst, M. Heyns, M. Caymax, I. Radu and A. Delabie, *J. Chem. Phys.*, 2019, **150**, 104703.
- 14 J. Park, M. S. Kim, E. Cha, J. Kim and W. Choi, *Sci. Rep.*, 2017, **7**, 1–8.
- 15 K. M. McCreary, A. T. Hanbicki, G. G. Jernigan, J. C. Culbertson and B. T. Jonker, *Sci. Rep.*, 2016, **6**, 19159.
- 16 B. Groven, A. N. Mehta, H. Bender, Q. Smets, J. Meersschaut, A. Franquet, T. Conard, T. Nuytten, P. Verdonck, W. Vandervorst, M. Heyns, I. Radu, M. Caymax and A. Delabie, *J. Vac. Sci. Technol., A*, 2018, **36**, 01A105.
- 17 K. Kang, S. Xie, L. Huang, Y. Han, P. Y. Huang, K. F. Mak, C.-J. Kim, D. Muller and J. Park, *Nature*, 2015, **520**, 656–660.
- 18 G. Piccinini, S. Forti, L. Martini, S. Pezzini, V. Miseikis, U. Starke, F. Fabbri and C. Coletti, *2D Mater.*, 2019, **7**, 014002.
- 19 A. O. Tanoh, J. Alexander-Webber, J. Xiao, G. Delpont, C. A. Williams, H. Bretscher, N. Gauriot, J. Allardice, R. Pandya, Y. Fan, Z. Li, S. Vignolini, S. D. Stranks, S. Hofmann and A. Rao, *Nano Lett.*, 2019, **19**, 6299–6307.
- 20 F. Wang, S. Li, M. A. Bissett, I. A. Kinloch, Z. Li and R. J. Young, *2D Mater.*, 2020, **7**, 045022.
- 21 X. Zhang, H. Nan, S. Xiao, X. Wan, X. Gu, A. Du, Z. Ni and K. K. Ostrikov, *Nat. Commun.*, 2019, **10**, 598.
- 22 P. Yang, X. Zou, Z. Zhang, M. Hong, J. Shi, S. Chen, J. Shu, L. Zhao, S. Jiang, X. Zhou, Y. Huan, C. Xie, P. Gao, Q. Chen, Q. Zhang, Z. Liu and Y. Zhang, *Nat. Commun.*, 2018, **9**, 979.
- 23 S. Husain, A. Kumar, P. Kumar, A. Kumar, V. Barwal, N. Behera, S. Choudhary, P. Svedlindh and S. Chaudhary, *Phys. Rev. B*, 2018, **98**, 180404(R).
- 24 S. Husain, X. Chen, R. Gupta, N. Behera, P. Kumar, T. Edvinsson, F. García-Sánchez, R. Brucas, S. Chaudhary, B. Sanyal, P. Svedlindh and A. Kumar, *Nano Lett.*, 2020, **20**, 6372–6380.
- 25 J. Tao, J. Chai, X. Lu, L. M. Wong, T. I. Wong, J. Pan, Q. Xiong, D. Chi and S. Wang, *Nanoscale*, 2015, **7**, 2497–2503.
- 26 Y. Koçak and E. Gür, *ACS Appl. Mater. Interfaces*, 2020, **13**, 15785–15792.
- 27 M. Regula, C. Ballif, J. Moser and F. Lévy, *Thin Solid Films*, 1996, **280**, 67–75.
- 28 K. Ellmer, C. Stock, K. Diesner and I. Sieber, *J. Cryst. Growth*, 1997, **182**, 389–393.
- 29 K. Ellmer, S. Seeger, I. Sieber, W. Bohne, J. Röhrich, E. Strub and R. Mientus, *Phys. Status Solidi A*, 2006, **203**, 497–503.
- 30 M. M. S. Villamayor, A. Lindblad, F. O. Johansson, T. Tran, N. H. Pham, D. Primetzhofer, N. L. Sorgenfrei, E. Giangrisotomi, A. Föhlisch, P. Lourenço, R. Bernard, N. Witkowski, G. Prévot and T. Nyberg, *Vacuum*, 2021, **188**, 110205.



- 31 H. Terrones, E. Del Corro, S. Feng, J. Poumirol, D. Rhodes, D. Smirnov, N. Pradhan, Z. Lin, M. Nguyen, A. Elias, *et al.*, *Sci. Rep.*, 2014, **4**, 4215.
- 32 A. Berkdemir, H. R. Gutiérrez, A. R. Botello-Méndez, N. Perea-López, A. L. Elías, C.-I. Chia, B. Wang, V. H. Crespi, F. López-Urías, J.-C. Charlier, *et al.*, *Sci. Rep.*, 2013, **3**, 1–8.
- 33 W. Zhao, Z. Ghorannevis, K. K. Amara, J. R. Pang, M. Toh, X. Zhang, C. Kloc, P. H. Tan and G. Eda, *Nanoscale*, 2013, **5**, 9677–9683.
- 34 N. Peimyoo, J. Shang, W. Yang, Y. Wang, C. Cong and T. Yu, *Nano Res.*, 2015, **8**, 1210–1221.
- 35 H. Zeng, G.-B. Liu, J. Dai, Y. Yan, B. Zhu, R. He, L. Xie, S. Xu, X. Chen, W. Yao, *et al.*, *Sci. Rep.*, 2013, **3**, 1–5.
- 36 D. M. Popovic, V. Milosavljevic, A. Zekic, N. Romcevic and S. Daniels, *Appl. Phys. Lett.*, 2011, **98**, 051503.
- 37 M. P. Seah, *Surf. Interface Anal.*, 2001, **31**, 721–723.
- 38 A. Berkdemir, H. R. Gutiérrez, A. R. Botello-Méndez, N. Perea-López, A. L. Elías, C. I. Chia, B. Wang, V. H. Crespi, F. López-Urías, J. C. Charlier, H. Terrones and M. Terrones, *Sci. Rep.*, 2013, **3**, 1–8.
- 39 A. A. Mitioglu, P. Plochocka, G. Deligeorgis, S. Anghel, L. Kulyuk and D. K. Maude, *Phys. Rev. B: Condens. Matter Mater. Phys.*, 2014, **89**, 245442.
- 40 W. Shi, M.-L. Lin, Q.-H. Tan, X.-F. Qiao, J. Zhang and P.-H. Tan, *2D Mater.*, 2016, **3**, 025016.
- 41 M. R. Molas, K. Nogajewski, M. Potemski and A. Babiński, *Sci. Rep.*, 2017, **7**, 1–8.
- 42 M. O'Brien, N. McEvoy, D. Hanlon, T. Hallam, J. N. Coleman and G. S. Duesberg, *Sci. Rep.*, 2016, **6**, 19476.
- 43 Z. He, X. Wang, W. Xu, Y. Zhou, Y. Sheng, Y. Rong, J. M. Smith and J. H. Warner, *ACS Nano*, 2016, **10**, 5847–5855.
- 44 F. Zhang, Y. Lu, D. S. Schulman, T. Zhang, K. Fujisawa, Z. Lin, Y. Lei, A. L. Elias, S. Das, S. B. Sinnott, *et al.*, *Sci. Adv.*, 2019, **5**, eaav5003.
- 45 L. Yuan and L. Huang, *Nanoscale*, 2015, **7**, 7402–7408.
- 46 Z. He, Y. Sheng, Y. Rong, G.-D. Lee, J. Li and J. H. Warner, *ACS Nano*, 2015, **9**, 2740–2748.
- 47 D. Thakur, P. Kumar, M. Sabarigresan, R. Ramadurai and V. Balakrishnan, *Surf. Interfaces*, 2021, **26**, 101308.
- 48 X. Xu, L. Li, X. Li, X. Hu, M. Yang, Q. Guo, Y. Wang, X. Zhuang and B. Liang, *Optik*, 2022, **251**, 168374.
- 49 J. Sundberg, R. Lindblad, M. Gorgoi, H. Rensmo, U. Jansson and A. Lindblad, *Appl. Surf. Sci.*, 2014, **305**, 203–213.
- 50 D. S. Jensen, S. S. Kanyal, N. Madaan, M. A. Vail, A. E. Dadson, M. H. Engelhard and M. R. Linford, *Surf. Sci. Spectra*, 2013, **20**, 36–42.
- 51 G. Greczynski and L. Hultman, *Sci. Rep.*, 2021, **11**, 1–5.
- 52 J. C. Fuggle and N. Mårtensson, *J. Electron Spectrosc. Relat. Phenom.*, 1980, **21**, 275–281.
- 53 J.-J. Pireaux, J. Ghijsen, J. W. McGowan, J. Verbist and R. Caudano, *Surf. Sci.*, 1979, **80**, 488–502.
- 54 D. David, C. Godet, F. O. Johansson and A. Lindblad, *Appl. Surf. Sci.*, 2020, **505**, 144385.
- 55 J. You, M. D. Hossain and Z. Luo, *Nano Convergence*, 2018, **5**, 26.
- 56 2H Tungsten Disulfide, <http://www.hqgraphene.com/WS2.php>.
- 57 A. J. Ying, C. E. Murray and I. Noyan, *J. Appl. Crystallogr.*, 2009, **42**, 401–410.

